NUMERICAL INVESTIGATION OF MIXED MAGNETO-HYDRODYNAMIC CONVECTION IN A LID-DRIVEN CUBIC CAVITY WITH A HYBRID NANOFLUID

Abderrahim BAHOUM [1,*], Mohamed EL HATTAB[1], Youness EL HAMMAMI[2,1]

[*1] Laboratory of Mechanics, Processes, Energy and Environment (LMPEE), Ibn Zohr University, ENSA Agadir, Morocco.

[2] Laboratory of Artificial Intelligence, Data Sciences and Emerging Systems, Sidi Mohammed Ben Abdellah University, ENSA Fez, Morocco.

[*] Corresponding author; E-mail: abderrahim.bahoum@edu.uiz.ac.ma

This study presents a numerical investigation on the mixed magneto-hydrodynamic (MHD) convection of a hybrid Cu-Al_2O_3-water nanofluid within a driven-wall cubic cavity. An isothermal block at temperature T_h is positioned on the left wall of the cavity, while the right wall is maintained at a temperature T_c ($<T_h$). An inclined magnetic field is applied to the entire system. The finite volume method, combined with the SIMPLE algorithm for velocity-pressure coupling, was adopted to solve the governing equations. Parameters such as Reynolds number (Re) (50:200), Richardson number (Ri) (0.01:100), Hartmann number (Ha) (0:100), magnetic field tilt angle (γ) (0°:90°), and nanoparticle volume fraction (Φ) (0:0.06) were examined. Observations are illustrated through streamlines, isotherms, velocity profiles, and average Nusselt number. The results show that increasing the Reynolds number (Re), Richardson number (Ri) and nanoparticle volume fraction (Φ) improves heat transfer within the cavity. Conversely, an increase in the Hartmann number (Ha) has an unfavorable effect on heat transfer.

Key words*: Mixed convection, Hybrid nanofluid, magnetic field, lid-driven*

1. Introduction

Mixed convection is a heat transfer process that combines the mechanisms of natural and forced convection. In this phenomenon, the movement of the fluid is influenced both by the difference in density, due to the temperature gradient, and by an external source such as a fan, pump or moving wall, which imposes a flow. Studies of mixed convection in cubic cavities, both experimentally and numerically, have attracted increasing attention in recent decades, stimulated by their vast areas of application. Cavities of this type are being introduced into satellite technology [1], optical design [2], electronic devices [3], transformer thermal management [4], nuclear reactors [5], combustion engines [6], liquid-based solar heating systems [7], heat exchangers [8], thermal processes in the food industry [9, 10], and melting and solidification processes [11], among many others. Benderradji *et al.* [12] carried out a numerical study of mixed convection heat exchange in a cubic cavity, They revealed a transition between a structure dominated by natural convection at low Reynolds number and a structure dominated by forced convection at high Reynolds number. Later, Eutamene *et al.* [13]

studied the heat transfer characteristics of transient laminar mixed convection in driven lid cavities and showed how the dominant convection regime affected heat transfer. Also, Cárdenas *et al.* [14] carried out an experimental study of heat transfer by mixed opposite convection in open cubic cavities and revealed the oscillatory behaviour of flow and temperature distribution as a function of channel orientation and buoyancy force. Abdelmassih *et al.* [15] investigated stable and unstable mixed convection in a cubic cavity and identified complex flow behaviours as a function of Reynolds and Richardson numbers. Ghachem *et al.* [16] analysed heat and mass transfer in a lid-driven cavity and explored the effect of the direction of lid motion on heat and mass transfer.

The thermal conduction capacity of fluids is crucial in the fields of engineering, technology, and industry, where efficient heat transfer is essential for the proper functioning of equipment. Traditional fluids such as water, ethylene glycol, kerosene, and engine oils, despite their widespread use, offer limited thermal conductivity, thus limiting their ability to effectively dissipate heat from systems. In contrast, metallic materials, known for their excellent thermal conductivity, offer a promising solution to this limitation. The innovation is in dispersing metallic particles, oxides, and carbon with nanometric dimensions (1 to 100 nm) into traditional fluids, resulting in the creation of nanofluids [17]. These, due to their superior thermal conductivity, facilitate a more efficient heat transfer. The applications of nanofluids extend to various fields, such as heat exchangers [18], automotive industry [19], solar energy [20], and even medicine [21], thus benefiting from their improved performance. Karbasifar *et al.* [22] explored mixed convection in a lid-driven cavity containing a heated central elliptical cylinder, using a water-aluminium oxide (Al_2O_3) nanofluid. They found that increasing the Richardson number reduced the Nusselt number and the nanofluid velocity, while increasing the temperature difference enhanced the heat transfer and the Nusselt number. Meanwhile, Selimefendigil *et al.* [23] analysed mixed convection of nanofluids in a three-dimensional cavity with two rotating adiabatic circular cylinders. They found that the water-Cu nanofluid provided the highest heat transfer rate. Also, Al-Rashed *et al.* [24] performed three-dimensional numerical simulations on a cubic cavity using the finite volume method, focusing on the impact of the addition of nanoparticles on heat transfer and entropy generation. They found that the effect was limited for small hot blocks and low Richardson numbers. Later, Zhou *et al.* [25] studied the mixed convection heat transfer of the water-Al_2O_3 nanofluid in an entrained double-lid cubic cavity using the lattice Boltzmann method. They observed that nanoparticle volume fractions, Reynolds number, and Richardson number had large effects on heat transfer.

Mixed convection in the presence of magnetic fields has become a focal point of engineering challenges, especially in the field of cooling systems. At the same time, the number of studies into magnetohydrodynamic convection has grown steadily recently. For instance, Sheikholeslami *et al.* [26] presented the hydrothermal treatment of magnetohydrodynamic nanofluids in a cubic cavity heated from below. They observed that the application of a magnetic field caused a force opposite to the direction of flow, thus reducing convection currents. In addition, the Nusselt number increased with the Rayleigh number and the nanofluid volume fraction, but decreased with the Hartmann number. Also, Selimefendigil *et al.* [27] carried out a study of mixed convection in an entrained cavity filled with CuO-water nanofluids, under the influence of inclined magnetic fields. The results showed that the addition of nanoparticles increased local and mean heat transfer. Recently, Dey *et al.* [28] explored the effect of rotational magnetic fields on heat transfer in a square cavity using ferromagnetic and non-magnetic nanofluids. The experiment showed optimal heat transfer performance at a

nanoparticle concentration of 0.1% for both types of nanofluids, with superior performance of the ferromagnetic nanofluid in the absence of a rotating magnetic field. At the same time, Rehman *et al.* [29] carried out a numerical analysis on the magnetised ferric oxide nanofluid in a square cavity with a thread around a rotating heated cylinder. They showed that increasing the volume fraction of ferroparticles and their angular velocity improved the mean Nusselt number and decreased the viscous and thermal entropy. Gibanov *et al.* [30] focused on the mixed convection of Al_2O_3-water nanofluid suspension in a closed chamber with a movable top wall and a constant semicircular heat source, considering the impacts of thermal radiation and a uniform horizontal magnetic field. They revealed that efficient energy removal could be achieved under the influence of a magnetic field and the addition of nanoparticles. Shehata *et al.* [31] used computational analysis to examine the effects of introducing nanoparticles into a square cavity with a moving lid to enhance mixed hydro-magnetic convection. They found that increasing the percentage of solid volume enhanced heat transfer and that the magnetic field reduced the movement of heat and fluid. Further investigations were reported in references [32–39].

On the other hand, hybrid nanofluids, composed of two types of nano-additives or a stable mixture of composite nanoparticles in a base fluid, represent an evolution of classical nanofluids. They offer exceptional physicochemical properties, absent in individual nanoparticles, thanks to the synergistic effect between different particles. Hybrid nanofluids aim to improve thermal conductivity, stability, mechanical resistance, and heat transfer efficiency in various solar applications and other technical fields, thus marking their superiority and innovative nature. Sundar *et al.* [40] studied the flow of hybrid nanofluids in a tube with and without a magnetic field, using hybrid nanoparticles composed of $CoFe_2O_4$ and $BaTiO_3$. They observed an increase in the Nusselt number of up to 22.19% with 1.0% vol. of nanofluid without a magnetic field, and an increase of up to 72.33% with a magnetic field of 4000 G. Acharya [41] explored the practical applications of cubic cavities and the effect of internal obstacles and thermal modes on heat transfer. The study focused on an Ag-MgO hybrid nanofluid magnetized in a cubic cavity with an internal cylinder and showed that the Rayleigh number increased energy transport, while the magnetic factor reduced it.

Against this rich background, the present work aims to fill some existing gaps by investigating the mixed MHD convection of a Cu-Al_2O_3-water hybrid nanofluid within a cubic cavity with a movable top wall. A heating block of fixed temperature T_h is placed in the middle of the left wall of the cavity. The study focuses on the influence of several key parameters, such as Reynolds number, Richardson number, Hartmann number, magnetic field tilt angle, and nanoparticle volume fraction on the thermal and dynamic patterns. Unlike previous studies, this work introduces the combined effects of hybrid nanofluids, a movable boundary, and an oblique magnetic field, offering new insights into optimizing heat transfer in complex geometries.

2. Physical model and mathematical formulation

Figure 1 illustrates the geometric configuration of the problem under study. A three-dimensional cubic cavity of dimension L. Except for the right wall, maintained at a fixed cold temperature T_c, all walls of this cavity are adiabatic. An isothermal block, heated to a temperature T_h, is positioned in the middle of the left wall. The dimensions of this block are: h, e, and L, where $h = e = 0.2 \times L$. The cavity's top lid is moving at a constant speed U_0, moving in the positive direction of the X-axis. The cavity is filled with a water-based (Pr = 6.82) hybrid nanofluid containing Al_2O_3 and Cu nanoparticles

(50% Al_2O_3, 50% Cu). The assembly is exposed to a magnetic field inclined at an angle γ to the X axis. The Lorentz force $\vec{F} = \vec{J} \times \vec{B}$ arises when the conducting nanofluid interacts with an electromagnetic field. In this expression, $\vec{J}$ indicates the electric current density obtained according to Ohm's law, where the contribution of Coulomb's force is considered negligible: $\vec{J} = \sigma_{nf}\,(\vec{E} + \vec{V} \times \vec{B})$. The term $\vec{V}$ $(\vec{V} = u\,\vec{\imath} + v\,\vec{\jmath} + w\,\vec{k})$ represents the velocity vector, and $\vec{E}$ describes the electric field. Furthermore, the influence of electric fields, whether imposed or induced, is assumed to be negligible. Thus, the components of the Lorentz force have been established in the x, y, and z axes as follows:

$$\left.\begin{aligned} F_x &= \sigma_{nf} B_0^2 (v\,cos(\gamma)\sin(\gamma) - u\,sin^2(\gamma)) \\ F_y &= \sigma_{nf} B_0^2 (u\,cos(\gamma)\sin(\gamma) - v\,cos^2(\gamma)) \\ F_z &= -\sigma_{nf} B_0^2\, w \end{aligned}\right\} \quad (1)$$

Furthermore, the magnetic field induced by the movement of the electrically conductive hybrid nanofluid is considered negligible compared to the external magnetic field. Moreover, the Hall effect, viscous dissipation, velocity slip and radiation are also considered negligible. The base fluid and the small immersed particles are assumed to be in thermal equilibrium. And the hybrid nanofluid is supposed to be incompressible and Newtonian, and in laminar flow. Except for the density in the buoyancy term, which varies according to the Boussinesq approximation [42], all thermophysical properties (at 300K) listed in Tab. 1, are considered constant. Thus, based on the above assumptions [24, 31, 41], the dimensionless forms of the continuity, momentum and energy equations are as follows:

$$\frac{\partial U}{\partial X} + \frac{\partial V}{\partial Y} + \frac{\partial W}{\partial Z} = 0 \quad (2)$$

$$U\frac{\partial U}{\partial X} + V\frac{\partial U}{\partial Y} + W\frac{\partial U}{\partial Z} = -\frac{\partial P}{\partial X} + \frac{\nu_{nf}}{\nu_f}\frac{1}{Re}\left(\frac{\partial^2 U}{\partial X^2} + \frac{\partial^2 U}{\partial Y^2} + \frac{\partial^2 U}{\partial Z^2}\right) + \frac{\nu_{nf}}{\nu_f}\frac{Ha^2}{Re}(Vcos(\gamma)\,sin(\gamma) - Usin^2(\gamma)) \quad (3)$$

$$U\frac{\partial V}{\partial X} + V\frac{\partial V}{\partial Y} + W\frac{\partial V}{\partial Z} = -\frac{\partial P}{\partial Y} + \frac{\nu_{nf}}{\nu_f}\frac{1}{Re}\left(\frac{\partial^2 V}{\partial X^2} + \frac{\partial^2 V}{\partial Y^2} + \frac{\partial^2 V}{\partial Z^2}\right) + \frac{\nu_{nf}}{\nu_f}\frac{Ha^2}{Re}\left(Ucos(\gamma)\,sin(\gamma) - Vcos^2(\gamma)\right) + \frac{(\rho\beta)_{nf}}{\rho_{nf}\beta_f} Ri\,\theta \quad (4)$$

$$U\frac{\partial W}{\partial X} + V\frac{\partial W}{\partial Y} + W\frac{\partial W}{\partial Z} = -\frac{\partial P}{\partial Z} + \frac{\nu_{nf}}{\nu_f}\frac{1}{Re}\left(\frac{\partial^2 W}{\partial X^2} + \frac{\partial^2 W}{\partial Y^2} + \frac{\partial^2 W}{\partial Z^2}\right) - \frac{\nu_{nf}}{\nu_f}\frac{Ha^2}{Re}W \quad (5)$$

$$U\frac{\partial \theta}{\partial X} + V\frac{\partial \theta}{\partial Y} + W\frac{\partial \theta}{\partial Z} = \frac{\alpha_{nf}}{\alpha_f}\frac{1}{PrRe}\left(\frac{\partial^2 \theta}{\partial X^2} + \frac{\partial^2 \theta}{\partial Y^2} + \frac{\partial^2 \theta}{\partial Z^2}\right) \quad (6)$$

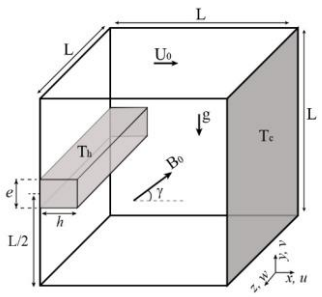

Figure 1: Physical model and coordinate system.

To nondimensionalize the previous equations, the following similarity variables are integrated:

$$X = \frac{x}{L}, Y = \frac{y}{L}, Z = \frac{z}{L}, U = \frac{u}{U_0}, V = \frac{v}{U_0}, W = \frac{w}{U_0}, P = \frac{p}{\rho_{nf} U_0^2}, \theta = \frac{T - T_c}{T_h - T_c} \quad (7)$$

$$Ri = \frac{Gr}{Re^2}, Gr = \frac{g\beta_f L^3 \Delta T}{\nu_f^2}, Re = \frac{LU_0}{\nu_f}, Pr = \frac{\nu_f}{\alpha_f}, Ha = B_0 L \sqrt{\frac{\sigma_{nf}}{\rho_{nf}\nu_{nf}}} \quad (8)$$

The nondimensional boundary conditions applied in this research are detailed as follows:

- The right wall maintains: $U = 0,\ V = 0,\ W = 0,\ \theta = 0$
- The top wall maintains: $U = 1,\ V = 0,\ W = 0,\ \frac{\partial \theta}{\partial Y} = 0$
- The heating block maintains: $U = 0,\ V = 0,\ W = 0,\ \theta = 1$
- Other walls of the cavity maintain: $U = 0,\ V = 0,\ W = 0,\ \frac{\partial \theta}{\partial n} = 0$

(9)

Where, *n* represents the normal direction to wall.

Table 2 presents the thermophysical characteristics of hybrid nanofluid.

Table 1: Thermophysical properties of nanoadditives and the base liquid [30, 43]**.**

Thermophysical properties	**Water**	**Cu**	**Al_2O_3**
Cp (J kg^{-1} K^{-1})	4179	385	765
ρ (kg m^{-3})	997.1	8933	3970
k (W $m^{-1}K^{-1}$)	0.613	401	40
β (K^{-1})	2.761×10^{-4}	1.67×10^{-5}	8.46×10^{-6}
α (m^2 s^{-1})	1.47×10^{-7}	-	-
σ(S m^{-1})	5×10^{-6}	5.96×10^{3}	10^{-10}

The calculation of the average Nusselt number on the block walls is based on the following relation:

$$Nu_{avg} = \frac{1}{Lh}\int_0^h \int_0^L -\frac{k_{nf}}{k_f}\left(\frac{\partial \theta}{\partial Y}\right)_{Y=Y_1} dZdX + \frac{1}{Le}\int_{Y_1}^{Y_2} \int_0^L -\frac{k_{nf}}{k_f}\left(\frac{\partial \theta}{\partial X}\right)_{X=h} dZdY + \frac{1}{Lh}\int_0^h \int_0^L -\frac{k_{nf}}{k_f}\left(\frac{\partial \theta}{\partial Y}\right)_{Y=Y_2} dZdX \quad (10)$$

Where $Y_1 = \frac{L-e}{2},\ Y_2 = \frac{L+e}{2}$

Table 2: Thermophysical correlations of usual hybrid nanofluid.

Properties	**Hybrid nanofluid (Cu-Al_2O_3-water)**
Density	$\rho_{nf} = (1-\Phi_s)\rho_f + \Phi_1\rho_1 + \Phi_2\rho_2$
Heat capacity	$(\rho C_p)_{nf} = (1-\Phi_s)(\rho C_p)_f + \Phi_1(\rho C_p)_1 + \Phi_2(\rho C_p)_2$
Viscosity [44]	$\mu_{nf} = \frac{\mu_f}{(1-\Phi_s)^{2.5}}$
Thermal conductivity [45]	$\frac{k_{nf}}{k_f} = \frac{(\Phi_1 k_1 + \Phi_2 k_2 + 2\Phi_s k_f) - 2\Phi_s(\Phi_s k_f - \Phi_1 k_1 - \Phi_2 k_2)}{(\Phi_1 k_1 + \Phi_2 k_2 + 2\Phi_s k_f) + \Phi_s(\Phi_s k_f - \Phi_1 k_1 - \Phi_2 k_2)}$
Thermal expansion coefficient	$(\rho\beta)_{nf} = (1-\Phi_s)(\rho\beta)_f + \Phi_1(\rho\beta)_1 + \Phi_2(\rho\beta)_2$

Electrical conductivity	$\sigma_{nf} = (1-\Phi_s)\sigma_f + \Phi_1\sigma_1 + \Phi_2\sigma_2$

3. Numerical method and validation

3.1. Numerical procedure

The code for solving the governing equations presented in the previous section is written in FORTRAN language. The governing equations are discretized by the finite volume method using the power law scheme. Then, the fully discretized equations are solved iteratively using a line-by-line Tri-Diagonal Matrix Algorithm procedure, TDMA [46]. The iterative process takes into account the pressure correction by implementing the SIMPLE algorithm [47], and reaches convergence when the variation of the dependent variables (*U*, *V*, *W*, *P* or θ) will be less than 10^{-6}. In order to stop the iterative process at convergence, a test is established at each step according to the following criterion:

$$\sum_{i,j,k=1}^{i_{max},j_{max},k_{max}} \frac{\left|\emptyset_{i,j,k}^{n+1} - \emptyset_{i,j,k}^{n}\right|}{\left|\emptyset_{i,j,k}^{n}\right|} \leq 10^{-6}$$

Where $\emptyset$ is one of the field variables (*U*, *V*, *W*, *T*, *P*) and *i*, *j* and *k* are the grid positions. *n* is the number of time steps.

3.2. Code validation and mesh study

A dimensional analysis of the mesh was conducted using grid sizes of 41^3, 51^3, 61^3, 71^3, and 81^3. The parameters defined for this study include Re = 200, Ri = 0.01, Ha = 25, $\gamma = 30°$, and $\Phi_1 = \Phi_2 = 0.02$. Following a mesh sensitivity test, a negligible difference was observed between the 61^3, 71^3 and 81^3 grids, (Tab. 3). So, during the simulations, a uniform spatial mesh in all directions of size 61^3 is adopted.

Table 3: Grid sensitivity test on Nu_{avg}.

Mesh size	**41×41×41**	**51×51×51**	**61×61×61**	**71×71×71**	**81×81×81**
Nu_{avg}	4.208	4.233	4.247	4.258	4.267
Dev(%)	--	0.59	0.33	0.25	0.21

To verify the calculation code, the results obtained are compared with those already available in the literature. Firstly, the results are compared with the work of Iwatsu *et al*. [48], which is based on a finite volume scheme for three-dimensional driven cavity flows, with an imposed vertical temperature gradient. The results of these comparisons are presented in Tab. 4, for the calculations of the average Nusselt number. Following the analysis, it is found that our results significantly agree with those of [48]. The second validation was performed by comparing our results with those of Bouchta *et al.*[43], Who numerically studied free MHD convection in a differentially heated cubic cavity filled with a Cu-water nanofluid with Pr = 6.2. Fig. 2 shows a good agreement between our average Nusselt number results and those obtained by Bouchta *et al*.[43].

Table 4: Nusselt Number Comparison: Ours Against [48]**.**

	Ri=0.001			**Ri=1**			**Ri=10**		
	Present	[48]	**Diff.**	**Present**	[48]	**Diff.**	**Present**	[48]	**Diff.**
Re=100	1.83	1.82	0.54%	1.35	1.33	1.5%	1.09	1.08	0.92%
Re=400	3.89	3.99	2.5%	1.48	1.50	1.33%	1.14	1.17	2.56%
Re=1000	6.94	7.03	1.28%	1.76	1.80	2.22%	1.29	1.37	5.83%

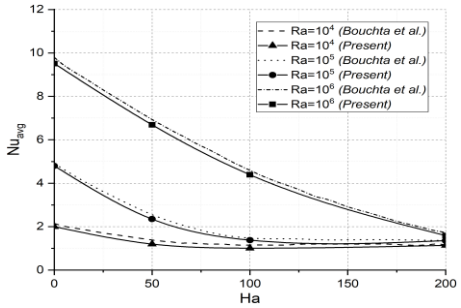

Figure 2: Comparison of the Nusselt number between the present and numerical results by Bouchta *et al.*[43], for Φ =5%.

4. Results and discussion

This segment presents numerical results from modelling the mixed convection of a Cu-Al_2O_3-water hybrid nanofluid within a three-dimensional cubic cavity with a moving wall. Various control parameters such as Ri, Re, Ha, γ and Φ are anticipated to demonstrate variations in the so-called isotherms, dynamic field, as well as heat transfer results. A thorough analysis is conducted to assess how different parameters affect the flow transition. The default parametric range is set to Re=100, Ri=1, Ha=25, Φ_s=0.04 and γ=30°.

4.1. Effect of Reynolds and Richardson numbers

The control parameters include the Richardson number ($Ri = Gr/Re^2$) and Reynolds number (Re) (Re=50, 100, 150 and 200). The results are presented in the form of streamlines and isotherms, covering three distinct regimes: the predominance of forced convection (Ri = 0.01), mixed convection (Ri = 1.0) and the predominance of natural convection (Ri = 10 and Ri = 100).

Figure 3 shows the variations in streamlines for different combinations of Reynolds and Richardson numbers. Initially at Ri=0.01, and for different values of Re, vortices form in a clockwise direction in the upper part of the cavity, mainly under the influence of the velocity of the upper lid, as shown in Fig. 3. However, for Re=50 and Re=100, the velocity of the nanofluid under the heat source (the lower part of the cavity) remains limited, and the influence of the lid on the nanofluid is confined to the upper half of the enclosure. As Re increases from 50 to 200, the size of the vortices increases and their center moves to the upper right-hand part of the cavity. The temperature curves, presented in Fig. 4, show that the isotherms in the lower half of the enclosure align parallel to the vertical walls at Re=50, indicating a predominance of thermal conduction. Despite the increase in Re from 50 to 200, the distance between isotherms remains large near the heating block, suggesting a relatively low heat transfer coefficient.

For the mixed convection regime with Ri = 1, the main vortex will occupy most of the cavity for all Re values. In addition, the movement of the upper wall begins to influence the entire nanofluid inside the cavity as Re gradually increases from 50 to 200. Furthermore, the isotherms, especially near the block, become closer together, indicating an improvement in heat exchange between the nanofluid and the block walls. Above Re=100, the isotherms become more inclined and almost horizontal, indicating that convection prevails throughout the cavity.

For Ri=10, where natural convection predominates, the center of the convective cell will be located near the driven top wall. This center shifts to the right with increasing Re. At Ri=100 and for Re=50, the patterns of the streamlines reveal an intense convective cell occupying the entirety of the cavity, rotating clockwise with its center located in the upper left corner (between the block and the moving wall), suggesting a predominance of intense natural convection. As the Reynolds number increases, the effect of the wall gradually takes control in the upper part of the enclosure, manifested by the movement of the convective cell's center to the right. On the other hand, by gradually changing the Reynolds number from 50 to 200 for Ri=10, the isotherms converge around the heating block. However, they align parallel to the horizontal walls in the rest of the cavity. Also, for Ri=100, a vertical stratification of the isotherms manifests throughout the cavity, with a notable concentration around the block walls, thus demonstrating a high rate of heat transfer. This general pattern of the isotherms is explained by the influence of buoyancy forces; the rising hot fluid is driven to the right by the moving top wall, while the cold fluid moves to the left after descending. The temperature along the region of the cold fluid increases again due to the heat source, thus causing the fluid to rise and the flow pattern to repeat.

Figure 5 shows the velocity profiles along the horizontal X direction at Y=Z=0.5 for various Richardson numbers (Ri). These profiles show an increase in velocity magnitude with increasing Richardson number for all values of Re. Moreover, the magnitude of the velocity is significantly higher for Ri=100 compared to the cases of Ri=0.01 and Ri=1, while the velocity exhibits a moderate magnitude for Ri=10. Furthermore, for a fixed value of Ri, the increase in Re leads to a slight increase in velocity at the minimum and maximum points, observed as a result of the clockwise flows. It is clear that natural convection favors the movement of the nanofluid throughout the enclosure more intensely than forced convection induced by the movement of the upper wall.

The effects of the Richardson number (Ri) and the Reynolds number (Re) on the average Nusselt number are presented in Fig. 6. Generally, at a given value of Reynolds (Re), the average Nusselt number increases with the elevation of the Richardson number. Moreover, irrespective of the Ri value, the increase in Re leads to a rise in the average Nusselt number. This increase reaches 97% when Re goes from 50 to 200, for a Ri=100. The main characteristics of the flow and temperature in the cavity, for Ri values of 0.01, 1, 10, or 100 and Re values of 50, 100, 150, or 200, are compared to Fig. 3 and Fig. 4 in order to explain the reason for the increase in heat transfer. A clockwise rotating vortex occupies the upper part of the cavity, limiting the convective heat exchange on the top wall and a portion of the block's right wall. In contrast, the movement of the nanofluid in the lower part of the cavity remains very limited, especially for low values of Re, with isotherms becoming more parallel to the vertical walls, indicating a quasi-conduction regime. This highlights the decrease in average heat transfer for low values of Ri (Ri=0.01 and Ri=1). As natural convection takes precedence (Ri=10 and Ri=100), the vortex begins to expand to occupy the entirety of the cavity. Thus, the movement of the

flow increases, especially for higher values of Re, promoting convection as the dominant mechanism of heat transfer, as demonstrated in Fig. 6.

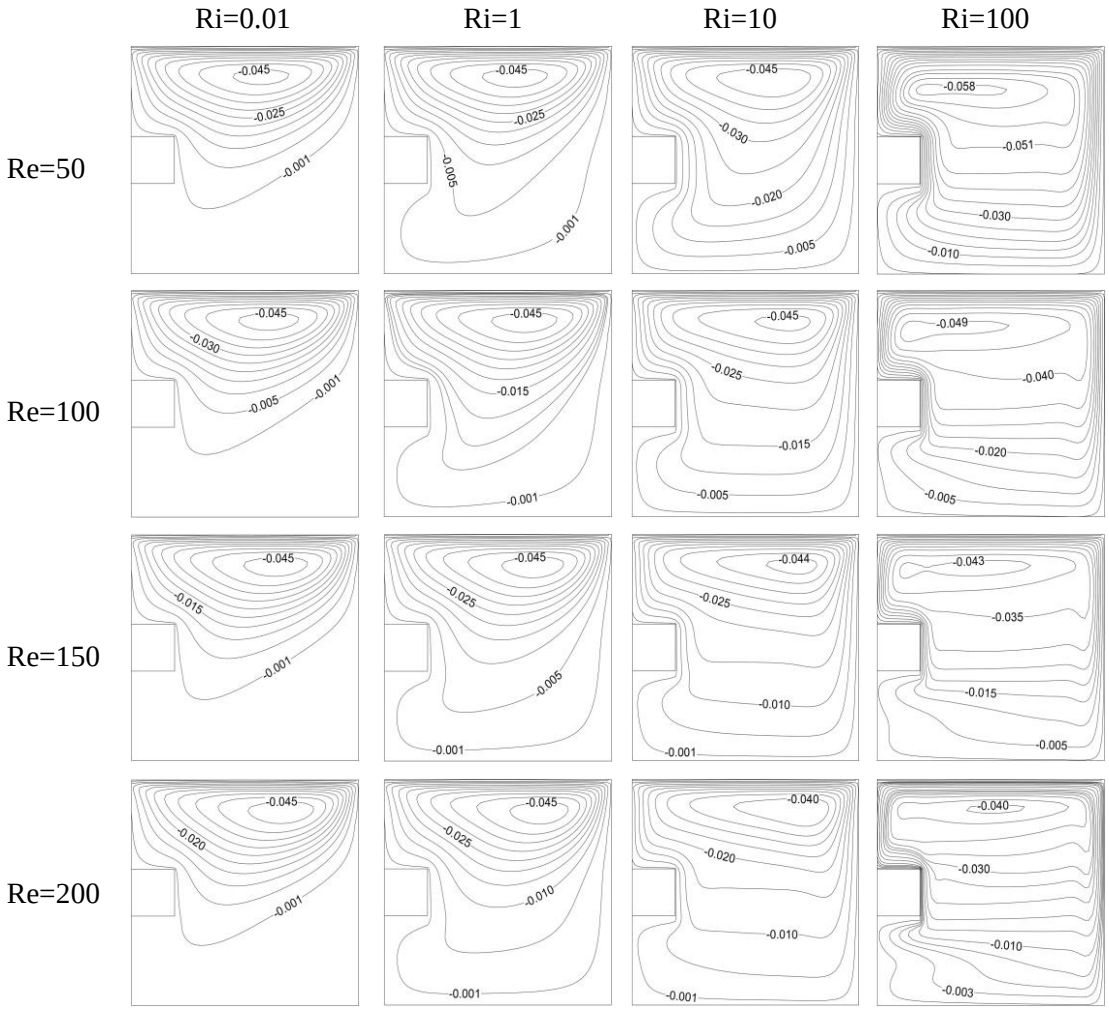

Figure 3: Streamlines at Z=0.5 for different values of Ri and Re.

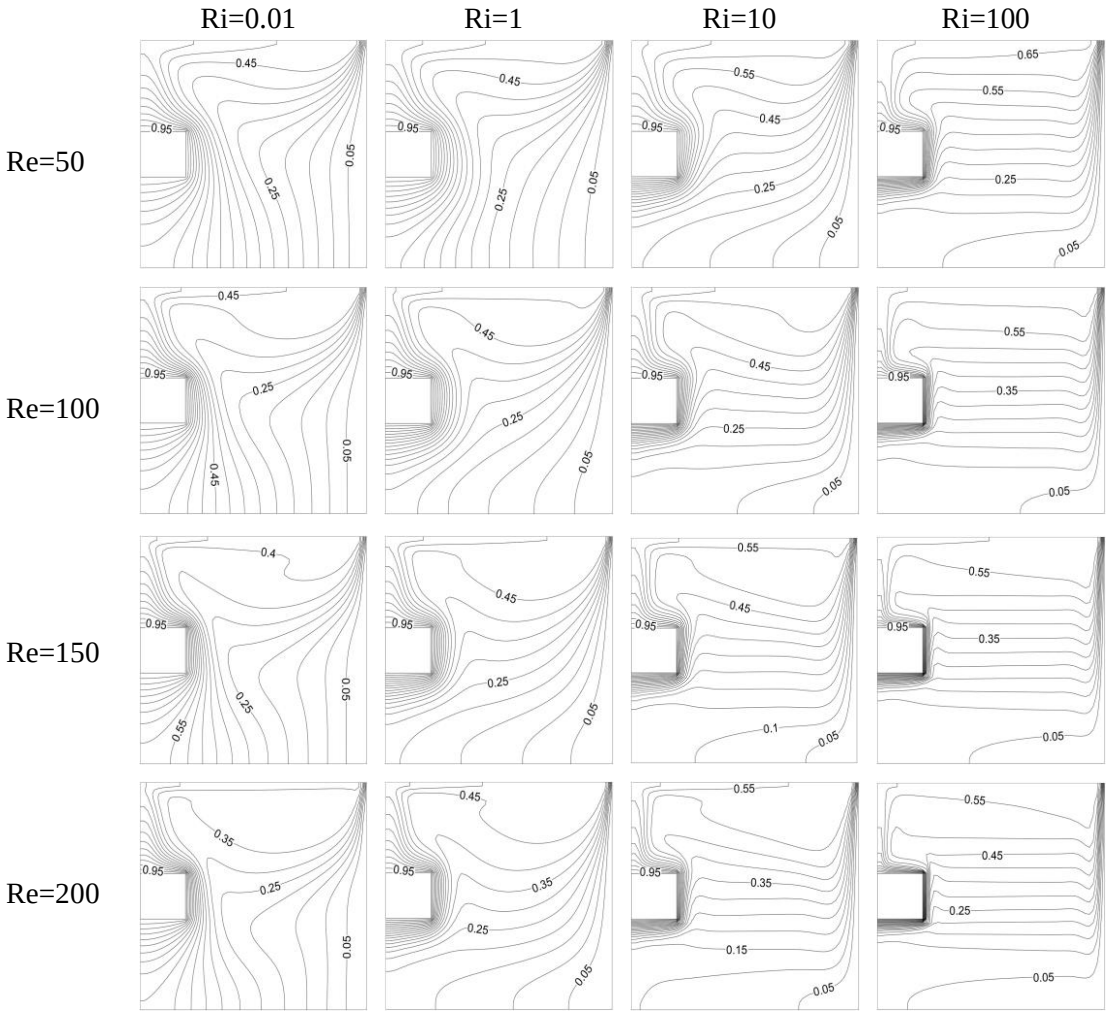

Figure 4: Isothermal lines at Z=0.5 for different values of Ri and Re.

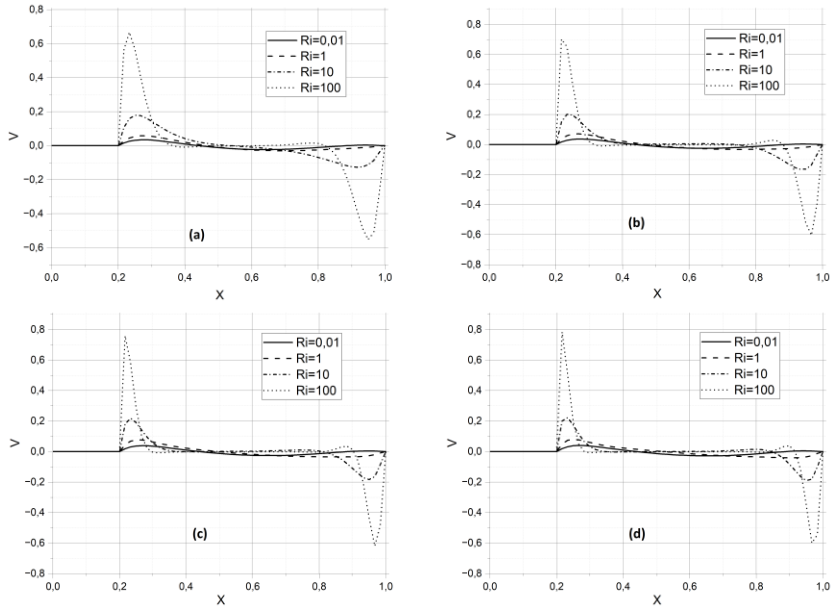

Figure 5: Vertical velocity profiles at Y = Z = 0.5 as a function of Ri for various Re values: (a) Re=50, (b) Re=100, (c) Re=150, (d) Re=200

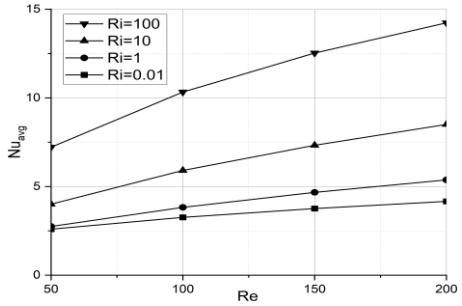

Figure 6: Variation of the Average Nusselt number as a function of Re and Ri.

4.2. Effect of the Hartmann number and the angle γ of magnetic field inclination

Figures 7 and 8 show the streamlines and isotherms for Ri = 1, Re = 100, and various values of Ha and γ. Across all γ values, the streamlines reveal that as the Hartmann number (Ha) increases, the damping effect of the magnetic field intensifies, reducing flow velocities and altering the dynamic structure within the cavity. Moreover, for a horizontally aligned magnetic field, the main convective cell divides into two vortices as Ha increases, indicating a decrease in the effect of convection with the strengthening of the magnetic field. Similarly, the isotherms reveal a quasi-conductive zone, indicating heat transfer primarily by conduction, except near the top cover where the effect of shear force alters this pattern. At γ = 30°, the inclination of the magnetic field begins to disrupt the flow symmetry. At Ha = 25, the streamlines are distorted, indicating a change in the flow dynamics due to the magnetic field component acting in a new direction. The isotherms show a relatively homogeneous temperature distribution. At Ha = 50, the oriented magnetic field allows the fluid to flow in oblique directions, while at Ha = 100, the fluid exhibits behavior similar to the case of γ = 0.

As the angle of inclination of the magnetic field increases up to 60°, the streamlines are clearly inclined, reflecting a significant change in flow compared to the previous inclination. What's more, the main vortex remains unicellular even at Ha=100, with a 75% decrease in the ψ_{max} value compared with that observed in the case where Ha = 25. Although the isotherms show a slight change in temperature gradient at the top of the right cavity wall, this temperature gradient decreases with increasing Ha to 50, and the isotherms demonstrate thermal stratification tilted towards the left wall at Ha = 100. A vertical magnetic field (γ = 90°) maximizes the suppressive effect on forced convection in the horizontal direction. This is generally due to the magnetic braking force, potentially enhancing vertical fluid stratification and promoting convection along the cavity sidewalls, while the isotherm lines show almost the same patterns as for γ = 60°.

Figure 9 shows the effect of magnetic field tilt angles on the average Nusselt number for different values of Ha. For all values of γ, increasing the magnetic field strength will reduce the heat transfer rate. However, as is evident, increasing the angle of magnetic inclination leads to an increase in the rate of heat transfer, irrespective of the values of Ha. This increase in rate is particularly noticeable when γ varies from 0° to 60°. On the other hand, from 60° to 90°, the change observed in the average Nusselt number is relatively minor. In order to explain this behaviour, Fig. 10 highlights the velocity profiles V as a function of X for various values of Ha and γ. This figure reveals that increasing the angle γ from 0° to 90° generates an increase in the amplitude of the fluid velocity for all values of the Hartmann number. At the same time, increasing the Hartmann number from 25 to 100 causes a

significant reduction in the amplitude of the velocity, so that at γ=90°, the rate of this reduction reaches 55% for Ha=100 compared with Ha=25. On the other hand, it is clear that the horizontal magnetic field significantly opposes fluid displacement due to the vertical component of the Lorentz force acting in the opposite direction to the Y axis. This opposition to the buoyancy force restricts the movement of the fluid in this direction, resulting in a reduction in the rate of heat transfer. This resistance is also reflected in the conduction pattern illustrated by the isothermal lines (Fig. 8), especially for high values of the Hartmann number. Conversely, the vertical magnetic field slows the movement of the fluid in the direction of the X axis, opposing the effect of the movable cover. This opposition attenuates the role of forced convection, leaving free convection to become the fluid's main driving force. This transition to free convection demonstrates increased heat transfer efficiency, explaining the remarkable increase in the average Nusselt number. In addition, the inclined magnetic field attenuates the influence of both buoyancy and shear forces on fluid displacement, albeit to a lesser extent than in previous cases.

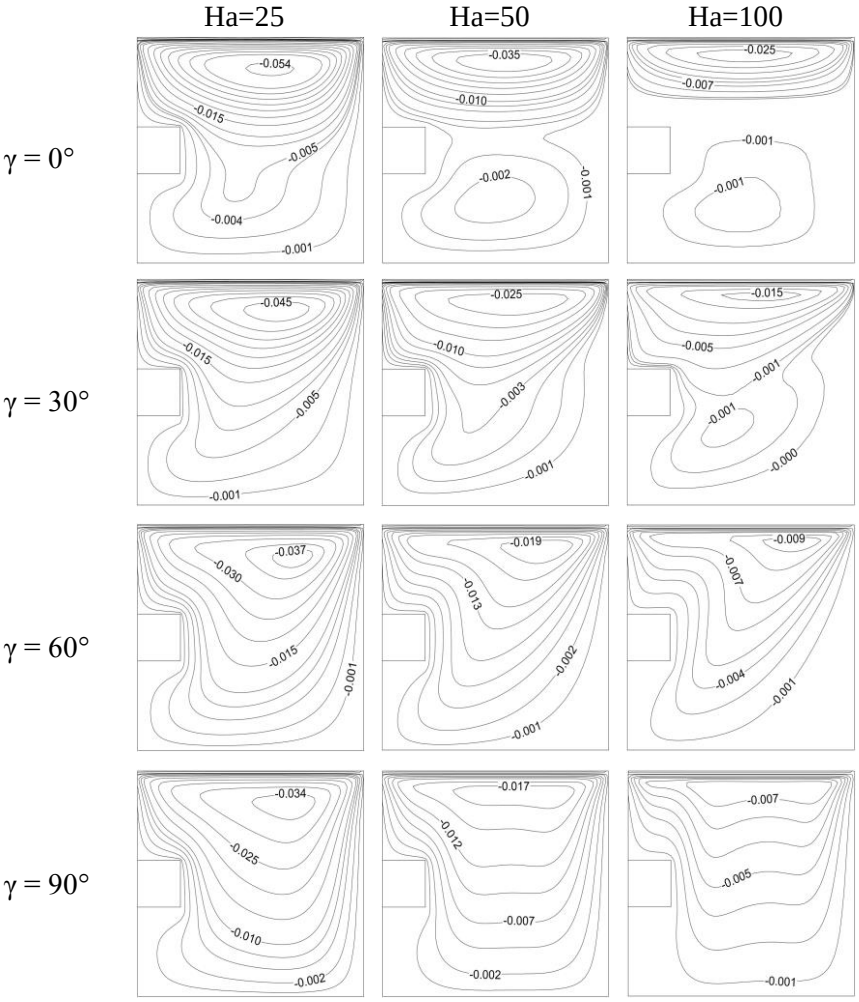

Figure 7: Streamlines at Z=0.5 for different values of Ha and γ.

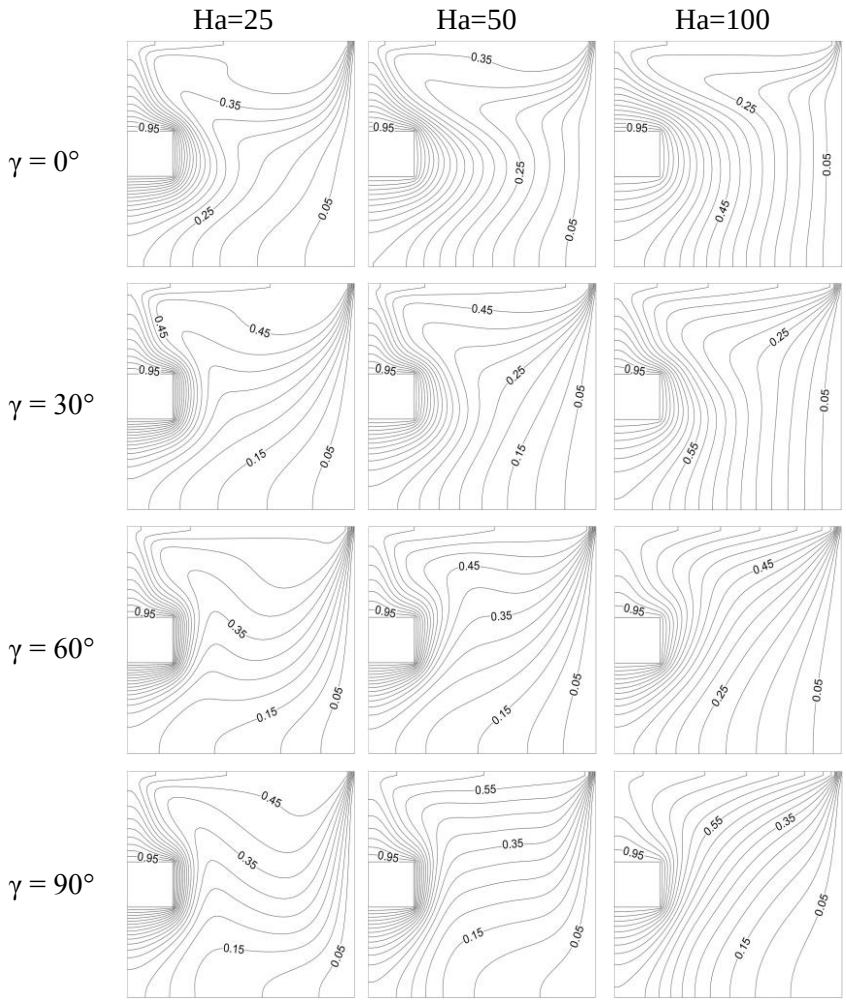

Figure 8: Isothermal lines at Z=0.5 for different values of Ha and γ.

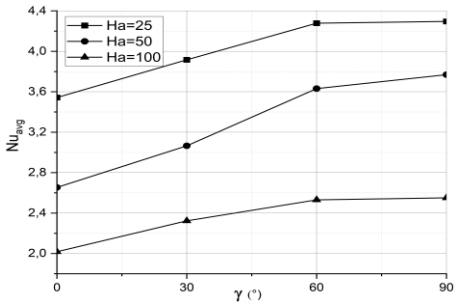

Figure 9: Variation of the Average Nusselt number as a function of γ and Ha.

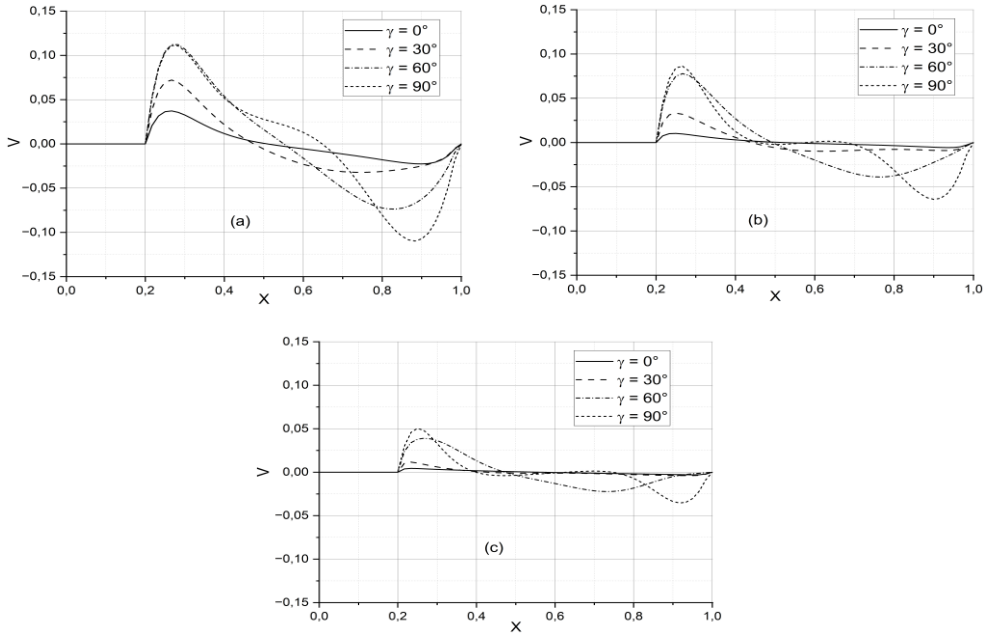

Figure 10: Vertical velocity profiles at Y = Z = 0.5 as a function of γ for various Ha values: (a) Ha=25, (b) Ha=50, (c) Ha=100.

4.3. Effect of nanoparticle concentrations

Figure 11 illustrates the evolution of the average Nusselt number with the increase in the volume fraction of nanoparticles in various nanofluids (Al_2O_3-water, Cu-water, and Al_2O_3-Cu-water) for Richardson numbers (Ri) ranging from 0.01 to 100. A systematic increase in the average Nusselt number is observed as the concentration of nanoparticles intensifies, a trend consistent across all Ri values. At Ri = 0.01 and Φ_s =0.06, the Cu-water nanofluid exhibits a 0.91% higher Nusselt number compared to the Al_2O_3-water nanofluid and a 0.43% higher Nusselt number compared to the Al_2O_3-Cu-water nanofluid. Similarly, at Ri = 1, the Cu-water Nusselt number surpasses that of Al_2O_3-water by 1.29% and Al_2O_3-Cu-water by 0.78%. This trend becomes even more pronounced at Ri = 10, where the Cu-water Nusselt number exceeds that of Al_2O_3-water by 1.56% and Al_2O_3-Cu-water by 0.92%, highlighting the significant impact of Cu on enhancing heat transfer compared to Al_2O_3 under these specific conditions, due to its better thermal conductivity. This trend remains significant at Ri=100 as long as Φ_s<0.04. Conversely, the performance of the Cu-Al_2O_3-water hybrid nanofluid becomes superior to that of the other nanofluids when Φ_s exceeds 0.04.

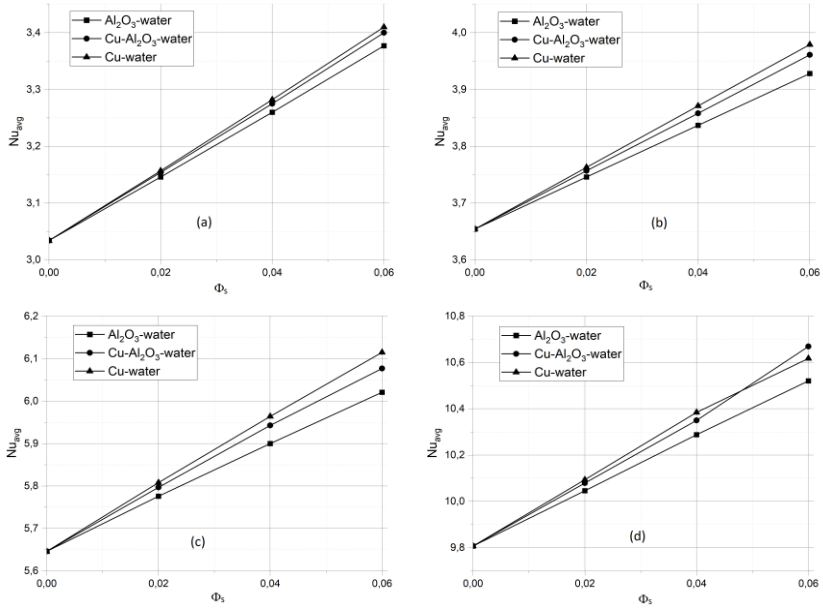

Figure 11: Variation of the Average Nusselt Number as a Function of Φ_s for Different Types of Nanofluid. (a) Ri=0.01; (b) Ri=1; (c) Ri=10; (d) Ri=100.

5. Conclusion

This research numerically investigates the mixed MHD convection of a Cu-Al_2O_3-water hybrid nanofluid within a cubic cavity with a moving top wall. All cavity walls are adiabatic except for the right wall, which is maintained at a cold temperature, Tc. An isothermal heating block, defined by its dimensions e, h, and L, is positioned in the middle of the left wall. The finite volume method is employed to solve the principal dimensionless equations. The study details how variables such as Re, Ri, Ha, γ, Φ_s, and the nanoparticle composition affect the hydrothermal behavior of the fluid and the heat transfer process within the cavity. Major conclusions drawn from the numerical analysis are summarized as follows:

- Increasing the Reynolds (Re) and Richardson (Ri) numbers enhances the heat transfer rate within the cavity; the regime dominated by natural convection promotes fluid circulation throughout the cavity. Furthermore, an increase in Re from 50 to 200 results in a 97% rise in the average Nusselt number (Nu_{avg}) for a Richardson number set at 100.
- An increase in the Hartmann number (Ha) from 25 to 100 leads to a slowdown in fluid movement within the cavity, and subsequently, a reduction in the heat transfer rate.
- For various Hartmann numbers (Ha), the gradual transition from a horizontal magnetic field to a vertical magnetic field results in a continuous increase in the average Nusselt number (Nu_{avg}).
- The average Nusselt number increases linearly with Φ_s for different types of nanofluid used, due to the enhancement of the fluid's thermal conductivity by adding nano-additives. Moreover, the Cu-water nanofluid shows the best thermal performance in various convection regimes, except in the case where Ri=100 and Φ_s>0.04, where the hybrid Cu-Al_2O_3-water nanofluid turns out to be the most efficient. This illustrates the advantage of using this hybrid nanofluid in similar situations.

Future research will focus on evaluating different types of nanoparticles to optimize heat transfer, adjusting the geometric parameters of the heat source, and analyzing the effect of a sinusoidal magnetic field on fluid behavior.

Nomenclature

B_0	Magnetic field strength, [T]	T	Dimensional temperature, [K]
C_p	Specific heat, [$JKg^{-1}K^{-1}$]	u, v, w	Dimensional velocity components, [ms^{-1}]
e	Thickness of the heating block, [m]	U, V, W	Dimensionless velocity components, [-]
g	Gravitational acceleration, [ms^{-2}]	x, y, z	Dimensional coordinates, [m]
h	Width of the heating block, [m]	X, Y, Z	Dimensionless coordinates, [-]
Ha	Hartmann number, [-]		*Greek letters*
k	Thermal conductivity, [$Wm^{-1}K^{-1}$]	α	Thermal diffusivity, [m^2s^{-1}]
L	Width of the enclosure, [m]	β	Coefficient of thermal expansion, [K^{-1}]
Nu	Nusselt number, [-]	γ	magnetic field inclination [degrees]
Pr	Prandtl number, [-]	μ	Dynamic viscosity, [Pas]
P	Pressure, [Pa]	ν	Kinematic viscosity, [m^2s^{-1}]
Re	Reynolds number, [-]	Φ_1	Cu volume fraction, [-]
Ri	Richardson number, [-]	Φ_2	Al_2O_3 volume fraction, [-]
Φ_s	Solid volume fraction ($\Phi_s = \Phi_1 + \Phi_2$)	f	Base fluid
ρ	Density, [Kgm^{-3}]	nf	Nanofluid
σ	Electrical conductivity, [$\Omega^{-1}m^{-1}$]	s	Solid
θ	Dimensionless temperature, [-]	Cu	particle 1
	Subscripts	Al_2O_3	particle 2
avg	Average		
c	Cold		
h	Hot		

References

[1] Argence, B., et al., Prototype Of An Ultra-Stable Optical Cavity For Space Applications, *Opt. Express*, *20* (2012), 23, pp. 25409

[2] Hill, I.R., et al., Dual-Axis Cubic Cavity For Drift-Compensated Multi-Wavelength Laser Stabilisation, *Opt. Express*, *29* (2021), 22, pp. 36758

[3] Ambreen, T., et al., Irreversibility And Hydrothermal Analysis Of The MWCNTs/GNPs-Based Nanofluids For Electronics Cooling Applications Of The Pin-Fin Heat Sinks: Multiphase Eulerian-Lagrangian Modeling, *Case Studies in Thermal Engineering*, *31* (2022), pp. 101806

[4] Si, W.-R., et al., Numerical Study Of Electromagnetic Loss And Heat Transfer In An Oil-Immersed Transformer, *Mathematical Problems in Engineering*, *2020* (2020), pp. 1-13

[5] Zheng, J., et al., Study On Natural Convection Heat Transfer In A Closed Cavity With Hot And Cold Tubes, *Science Progress*, *104* (2021), 2, pp. 003685042110209

[6] Ferrão Teixeira Alves, L.O., et al., Comparative Performance Analysis Of Internal Combustion Engine Water Jacket Coolant Using A Mix Of Al2O3 And CuO-Based Nanofluid And Ethylene Glycol, *Energy*, *250* (2022), pp. 123832

[7] Flores, J.J., et al., Thermal Performance Of A Cubic Cavity With A Solar Control Coating Deposited To A Vertical Semitransparent Wall, *Solar Energy*, *82* (2008), 7, pp. 588-601

[8] Keya, S.T., et al., Mixed Convection Heat Transfer In A Lid-Driven Enclosure With A Double-Pipe Heat Exchanger, *International Journal of Thermofluids*, *13* (2022), pp. 100131
[9] Datta, A.K., Teixeira, A.A., Numerically Predicted Transient Temperature And Velocity Profiles During Natural Convection Heating Of Canned Liquid Foods, *Journal of Food Science*, *53* (1988), 1, pp. 191-195
[10] Ghani, A.G.A., et al., Numerical Simulation Of Natural Convection Heating Of Canned Food By Computational ¯uid Dynamics, *Journal of Food Engineering*, (1999)
[11] Ghalambaz, M., et al., Melting Of Nanoparticles-Enhanced Phase-Change Materials In An Enclosure: Effect Of Hybrid Nanoparticles, *International Journal of Mechanical Sciences*, *134* (2017), pp. 85-97
[12] Benderradji, R., Numerical Study Three-Dimensional Of Mixed Convection In A Cavity: Influence Of Reynolds And Grashof Numbers, *ARFMTS*
[13] Eutamene, S., Unsteady Mixed Convection In A Cubic Lid-Driven Cavity Partially Heated From The Bottom, *ARFMTS*
[14] Cárdenas, V., et al., Experimental Study Of Buoyancy And Inclination Effects On Transient Mixed Convection Heat Transfer In A Channel With Two Symmetric Open Cubic Cavities With Prescribed Heat Flux, *International Journal of Thermal Sciences*, *140* (2019), pp. 71-86
[15] Abdelmassih, G., et al., Steady And Unsteady Mixed Convection Flow In A Cubical Open Cavity With The Bottom Wall Heated, *International Journal of Heat and Mass Transfer*, *101* (2016), pp. 682-691
[16] Ghachem, K., et al., Numerical Simulation Of Three-Dimensional Double Diffusive Convection In A Lid-Driven Cavity, *International Journal of Thermal Sciences*, *110* (2016), pp. 241-250
[17] Choi, S.U.S., Eastman, J., *Enhancing Thermal Conductivity Of Fluids With Nanoparticles*, 1995
[18] Tian, G., et al., Entropy Analysis And Mixed Convection Of Nanofluid Flow In A Pillow Plate Heat Exchanger In The Presence Of Porous Medium, *Alexandria Engineering Journal*, *82* (2023), pp. 541-556
[19] Kumar, A., Hassan, M.A., Heat Transfer In Flat Tube Car Radiator With CuO-MgO-TiO2 Ternary Hybrid Nanofluid, *Powder Technology*, *434* (2024), pp. 119275
[20] Mostafizur, R.M., et al., Properties Of Al2O3-MWCNT/Radiator Coolant Hybrid Nanofluid For Solar Energy Applications, *Energy Reports*, *8* (2022), pp. 582-591
[21] Enjavi, Y., et al., Chapter 19 - Application Of Nanofluids In Drug Delivery And Disease Treatment, in: *Nanofluids and Mass Transfer* (Eds. M.R. Rahimpour et al.), Elsevier, 2022, pp. 449-465
[22] Karbasifar, B., et al., Mixed Convection Of Water-Aluminum Oxide Nanofluid In An Inclined Lid-Driven Cavity Containing A Hot Elliptical Centric Cylinder, *International Journal of Heat and Mass Transfer*, *116* (2018), pp. 1237-1249
[23] Selimefendigil, F., Öztop, H.F., Mixed Convection Of Nanofluids In A Three Dimensional Cavity With Two Adiabatic Inner Rotating Cylinders, *International Journal of Heat and Mass Transfer*, *117* (2018), pp. 331-343
[24] Al-Rashed, A.A.A.A., et al., Mixed Convection And Entropy Generation In A Nanofluid Filled Cubical Open Cavity With A Central Isothermal Block, *International Journal of Mechanical Sciences*, *135* (2018), pp. 362-375
[25] Zhou, W., et al., Lattice Boltzmann Simulation Of Mixed Convection Of Nanofluid With Different Heat Sources In A Double Lid-Driven Cavity, *International Communications in Heat and Mass Transfer*, *97* (2018), pp. 39-46
[26] Sheikholeslami, M., Magnetohydrodynamic Nanofluid Forced Convection In A Porous Lid Driven Cubic Cavity Using Lattice Boltzmann Method, *Journal of Molecular Liquids*, *231* (2017), pp. 555-565
[27] Selimefendigil, F., et al., MHD Mixed Convection And Entropy Generation Of Nanofluid Filled Lid Driven Cavity Under The Influence Of Inclined Magnetic Fields Imposed To Its Upper And Lower Diagonal Triangular Domains, *Journal of Magnetism and Magnetic Materials*, *406* (2016), pp. 266-281
[28] Dey, D., Dash, S.K., An Experimental Investigation On The Nanofluids In A Cavity Under Natural Convection With And Without The Rotary Magnetic Field, *Heliyon*, *9* (2023), 11, pp. e22416
[29] Rehman, N., et al., Finite Element Analysis On Entropy Generation In MHD Iron(III) Oxide-Water NanoFluid Equipped In Partially Heated Fillet Cavity, *Journal of Magnetism and Magnetic Materials*, *565* (2023), pp. 170269

[30] Gibanov, N.S., et al., MHD Mixed Convection Of Nanofluid In A Cavity With Isothermal Local Heater Under An Influence Of Velocity Modulation Of Upper Cold Wall, *International Journal of Thermal Sciences, 192* (2023), pp. 108402
[31] Shehata, A.I., et al., Enhancement Of Mixed Convection In A Lid Driven Enclosure Based On Magnetic Field Presence With Nanofluid, *Advances in Mechanical Engineering*, *15* (2023), 2, pp. 168781322311571
[32] Ghasemi, K., Siavashi, M., Three-Dimensional Analysis Of Magnetohydrodynamic Transverse Mixed Convection Of Nanofluid Inside A Lid-Driven Enclosure Using MRT-LBM, *International Journal of Mechanical Sciences*, *165* (2020), pp. 105199
[33] Nouri, R., et al., Non-Newtonian Natural Convection In A Square Box Submitted To Horizontal Heat Flux And Magnetic Field, *Therm sci*, (2024), 00, pp. 79-79
[34] Kherroubi, S., et al., Effect Of The Second Outlet Location And The Applied Magnetic Field Within A Ventilated Cubic Cavity Crossed By A Nanofluid On Mixed Convection Mode: Best Configurations, *J Therm Anal Calorim*, *139* (2020), 3, pp. 2243-2264
[35] Ahmed, S., et al., Magnetohydrodynamic Convective Flow Of Nanofluid In Double Lid-Driven Cavities Under Slip Conditions, *Therm sci*, *25* (2021), 3 Part A, pp. 1703-1717
[36] Selimefendigil, F., Chamkha, A.J., MHD Mixed Convection Of Nanofluid In A Three-Dimensional Vented Cavity With Surface Corrugation And Inner Rotating Cylinder, *HFF*, *30* (2019), 4, pp. 1637-1660
[37] Hemmat, E., et al., Mixed Convection Of Functionalized DWCNT-Water Nanofluid In Baffled Lid-Driven Cavities, *Therm sci*, *22* (2018), 6 Part A, pp. 2503-2514
[38] Ogut, E., Magnetohydrodynamic Mixed Convection In A Lid-Driven Rectangular Enclosure Partially Heated At The Bottom And Cooled At The Top, *Therm sci*, *21* (2017), 2, pp. 863-874
[39] El Hadoui, B., Kaddiri, M., Enhancement Of Carbon Nanotubes/Kerosene Nanofluids On Mixed Convective Heat Transfer In Rectangular Enclosures, *International Journal of Thermofluids*, *24* (2024), pp. 100932
[40] Sundar, L.S., Ramana, E.V., Influence Of Magnetic Field Location On The Heat Transfer And Friction Factor Of CoFe2O4-BaTiO3/EG Hybrid Nanofluids In Laminar Flow: An Experimental Study, *Journal of Magnetism and Magnetic Materials*, *579* (2023), pp. 170837
[41] Acharya, N., Magnetized Hybrid Nanofluid Flow Within A Cube Fitted With Circular Cylinder And Its Different Thermal Boundary Conditions, *Journal of Magnetism and Magnetic Materials*, *564* (2022), pp. 170167
[42] Gray, D.D., Giorgini, A., The Validity Of The Boussinesq Approximation For Liquids And Gases, *International Journal of Heat and Mass Transfer*, *19* (1976), 5, pp. 545-551
[43] Bouchta, S., Feddaoui, M., Numerical Simulation Of Free Convection In A Three-Dimensional Enclosure Full Of Nanofluid With The Existence A Magnetic Field, *EJEE*, *22* (2020), 6, pp. 405-411
[44] BRINKMAN, H.C., The Viscosity of Concentrated Suspensions and Solutions | The Journal of Chemical Physics | AIP Publishing, https://pubs.aip.org/aip/jcp/article-abstract/20/4/571/73765/The-Viscosity-of-Concentrated-Suspensions-and?redirectedFrom=PDF
[45] MAXWELL, J.C., *A Treatise On Electricity And Magnetism*, Clarendon Press, U.K, 1891
[46] Patankar, S.V., *Numerical Heat Transfer And Fluid Flow*, Hemisphere Publishing Corporation, 1980
[47] Van Doormaal, J.P., Raithby, G.D., Enhancements Of The Simple Method For Predicting Incompressible Fluid Flows, *Numerical Heat Transfer*, *7* (1984), 2, pp. 147-163
[48] Iwatsu, R., Hyun, J.M., Three-Dimensional Driven-Cavity Flows With A Vertical Temperature Gradient, *International Journal of Heat and Mass Transfer*, *38* (1995), 18, pp. 3319-3328

Submitted 22.7.2024
Revised 16.12.2024.
Accepted 20.12.2024.